Rational Molecular Design of Efficient Yellow-Red Dendrimer TADF for Solution-Processed OLEDs: A Combined Effect of Substitution Position and Strength of the Donors

Changfeng Si,[a] Dianming Sun,[a] Tomas Matulaitis, [a] David B. Cordes,[a] Alexandra M. Z. Slawin,[a] Eli Zysman-Colman[a]**

[a] Organic Semiconductor Centre, EaStCHEM School of Chemistry, University of St Andrews, St Andrews, Fife, UK. KY16 9ST, Fax: +44-1334 463808; Tel: +44-1334 463826

Corresponding: eli.zysman-colman@st-andrews.ac.uk;

Key words: thermally activated delayed fluorescence, solution-processing, red OLED, dibenzo[a,c]phenazine, dendrimers

Abstract

The development of high-performance solution-processed red organic light-emitting diodes remains a challenge, particularly in terms of maintaining efficiency at high luminance. Here, we designed and synthesized four novel orange-red solution-processable TADF dendrimers, **2GCzBP**, **2DPACzBP**, **2FBP2GCz** and **2FBP2DPACz**. We systematically investigated the effect of substitution position and strength of donors on the opto-electronic properties. The reverse intersystem crossing rate constant (k_{RISC}) of the emitters having donors substituted at positions 11 and 12 of the dibenzo[*a,c*]phenazine (BP) is more than 10-times faster than that of compounds substituted having donors substituted at positions 3 and 6. Compound **2DPACzBP**, containing stronger donors than **2GCzBP**, exhibits a red-shifted emission and smaller singlet−triplet energy splitting, ΔE_{ST}, of 0.01 eV. The solution-processed OLED with 10 wt% **2DPACzBP** doped in mCP emitted at 640 nm and showed a maximum external quantum efficiency (EQE_{max}) of 7.8%, which was effectively maintained out to a luminance of 1000 cd m^{-2}. Such a device performance at relevant display luminance is among the highest for solution-processed red TADF OLEDs. The efficiency of the devices was improved significantly by using 4CzIPN as an assistant dopant in a hyperfluorescence (HF) configuration, where the **2DPACzBP** HF device shows an EQE_{max} of 20.0% at λ_{EL} of 605 nm and remains high at 11.8% at a luminance of 1000 cd m^{-2}, which makes this device one of the highest efficiency orange-to-red HF SP-OLEDs to date.

Introduction

Organic light-emitting diodes (OLEDs) are now commonplace in displays in mobile phones, smartwatches and televisions and have made inroads in the solid-state lighting and automotive markets.[1–6] Most OLEDs are fabricated using a vacuum deposition technology that employs a complicated multilayered device architecture that results in high production costs. An alternative strategy would be to fabricate the OLEDs using lower-cost solution-processing techniques such as ink-jet printing, which also would provide a much simpler route to the production of large-area displays.[7,8] To achieve comparable performance metrics as vacuum-deposited devices, the key requirement for the solution-processed (SP) OLEDs is the availability of high-performance solution-processable emitter materials. Thermally activated delayed fluorescence (TADF) materials have attracted much attention over the last decade as a replacement emitter materials for noble metal-based phosphorescent complexes in OLEDs as they are less expensive and do not incorporate scarce platinoid metals yet are equally capable of harvesting up to 100% of the excitons to produce light.[1,4,9] Although vacuum-deposited OLEDs with small molecule TADF emitters have shown outstanding efficiencies in devices across the visible spectrum, these compounds tend to crystallize and thus are not ideal for solution-processed film formation. Macromolecules, such as dendrimers or polymers, on the other hand are perfect candidates for SP-OLEDs because of their superior film-forming ability, excellent thermal and morphological stability, and high affinity for substrates.[10–14] Significant progress has been made in the development of green and blue solution-processable TADF materials, and their corresponding SP-OLEDs exhibit outstanding maximum external quantum efficiency (EQE_{max}) of over 20%.[10,11,15–19]

Despite these achievements, there is presently a dearth of examples of efficient solution-processable red TADF emitters where their photoluminescence quantum yield is frequently much lower than for green and blue because of the lower radiative rate constant, k_r, and higher non-radiative rate constant, k_{nr}, as a result of the energy gap law.[20–22] So far, there are only a few reports of relatively efficient red TADF emitters for SP-OLEDs (Figure **1a**). Zhang *et al.* reported an orange-red emitter **4t-BuCzTTR** by using thianthrene 5,5,10,10-tetraoxide as the acceptor, 3,6-di-*tert*-butyl-9*H*-carbazole (*t*Cz) as the donor and the resulting SP-OLEDs emitted at λ_{EL}= 592 nm and showed an EQE_{max} of 6.2%, which dropped to around ~4.0% at 1000 cd m^{-2} (EQE_{1000}).[23] A deep red wedge-shaped organic fluorophore, **2TPA-PPDC**, was reported by Zhang *et al.*, whose SP-OLEDs emitted at λ_{EL}= 670 nm and showed an EQE_{max} of 3.2%.[24] A similar red emitter, **DDTPACz-DCPP**, containing carbazole donors that are

additionally decorated with two TPA units was reported by Wang *et al.*[25] The solution-processed devices with **DDTPACz-DCPP** showed EQE_{max}/EQE_{1000} of 13.6/~4.0% at λ_{EL} of 646 nm. Zeng *et al.* reported a SP-OLED containing the orange-red emitter **NAI_R3** that contains an extended donor moiety and uses *tert*-butylbenzene groups to improve solubility, which emitted at λ_{EL}= 622 nm and showed an EQE_{max} of 22.5%, but the device also showed a significant efficiency roll-off with an EQE_{1000} of 3.4%.[26] Liu *et al.* developed a D–A–D type red TADF emitter **TAT-FDBPZ** (Figure **1a**) by combining a triazatruxene (TAT) donor and a fluorene-substituted dibenzo[*a,c*]phenazine (BP) as the acceptor. The SP-OLED with **TAT-FDBPZ** reached an EQE_{max} of 9.2% at λ_{EL}= 611 nm and showed a low efficiency roll-off (EQE_{1000}=7.4%). Using the same BP acceptor, Chen *et al.* developed a D-A type red emitter, **oDBBPZ-DPXZ** (Figure **1a**) using two PXZs as donor moieties. SP-OLEDs with **oDBBPZ-DPXZ** emitted at λ_{EL}= 612 nm, and showed an EQE_{max} of 18.5%; however, efficiency roll-off was severe (EQE_{1000}=~3.0%).[27] This survey of the state-of-the-art in red TADF SP-OLEDs reveals that BP can be used effectively in red emitter design due to its rigid, large π-conjugated system. However, the efficiency of SP-OLEDs using BP-based red emitters still lags behind vacuum-deposited red TADF OLEDs with emitters containing the BP moiety, especially at high luminance (Figure **1a**).[28,29]

Here, we address this issue by employing this rigid BP core as the acceptor and strategically introducing two different donor dendrons, GCz and DPACz at different positions about the acceptor. We thus report the development of four orange-red TADF dendrimers: 11,12-bis(3,3",6,6"-tetra-*tert*-butyl-9'*H*-[9,3':6',9"-tercarbazol]-9'-yl)dibenzo[*a,c*]phenazine (**2GCzBP**); 9,9'-(dibenzo[*a,c*]phenazine-11,12-diyl)bis(N^3,N^3,N^6,N^6-tetraphenyl-9*H*-carbazole-3,6-diamine) (**2DPACzBP**); 11,12-difluoro-3,6-bis(3,3",6,6"-tetra-*tert*-butyl-9'H-[9,3':6',9"-tercarbazol]-9'-yl)dibenzo[*a,c*]phena-zine (**2FBP2GCz**); and 9,9'-(11,12-difluorodibenzo[*a,c*]phenazine-3,6-diyl)bis(N^3,N^3,N^6,N^6-tetraphenyl-9*H*-carbazole-3,6-diamine) (**2FBP2DPACz**), Figure **1b**. We systematically investigated the effect of donor strength and regiochemistry on the optoelectronic properties of the emitters. The reverse intersystem crossing rate constants (k_{RISC}) of **2GCzBP** and **2DPACzBP** are more than 10 times faster than those of **2FBP2GCz** and **2FBP2DPACz**. **2DPACzBP**, containing stronger donors, exhibits a red-shifted emission and smaller singlet−triplet energy splitting, ΔE_{ST}, of 0.01 eV compared to **2GCzBP** which has weaker donors. The SP-OLED with **2DPACzBP** emitted at λ_{EL} = 640 nm, showing an EQE_{max} of 7.8% and an EQE_{1000} of 7.5%. The efficiency of the SP-OLEDs could be improved with the introduction of an assistant dopant, **4CzIPN**, in a

hyperfluorescence (HF) device configuration. The highest HF device used **2DPACzBP** as the terminal emitter and showed an EQE_{max} of 20.0% at λ_{EL} of 605 nm (EQE_{1000} of 11.8%).

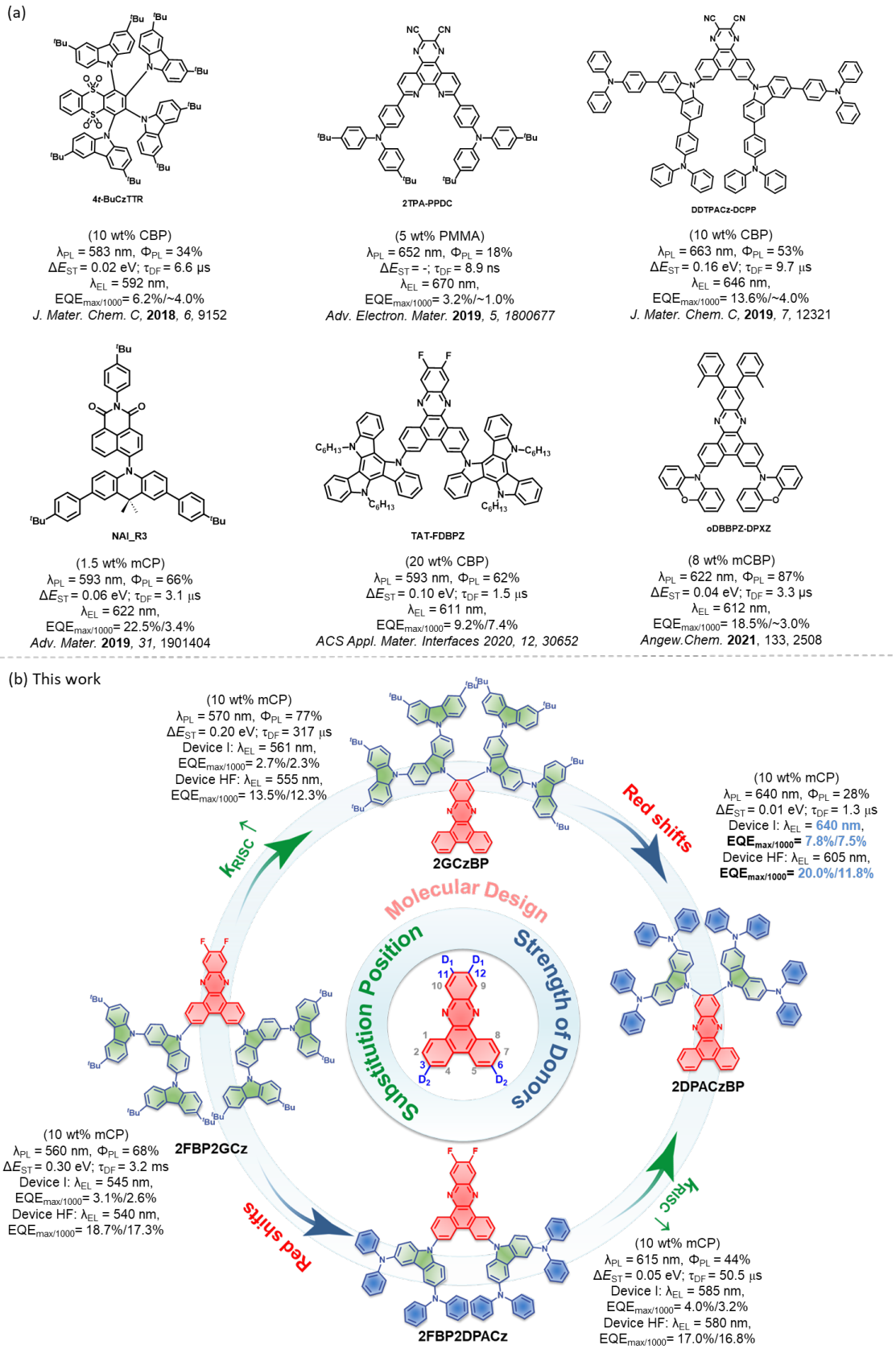

Figure **1**. (a) Reported solution-processable red TADF emitter materials. (b) Structures of the dendrimers **2GCzBP**, **2DPACzBP**, **2FBP2GCz** and **2FBP2DPACz** reported in this study based on bespoke second-generation tert-butylcarbazole (GCz), N^3,N^3,N^6,N^6-tetraphenyl-9H-carbazole-3,6-diamine (DPACz) donor and dibenzo[a,c]phenazine (BP) acceptor.

Results and Discussion

Synthesis

The synthetic routes for **2GCzBP**, **2DPACzBP**, **2FBP2GCz** and **2FBP2DPACz** are shown in Scheme **1**. Intermediate **1** was synthesized in 83% yield through the cyclization reaction of 4,5-difluorobenzene-1,2-diamine and phenanthrene-9,10-dione in 1-butanol. **2GCzBP** and **2DPACzBP** were synthesized with good yields (over 80%) through a nucleophilic aromatic substitution reaction between intermediate **1** and dendron GCz, or DPACz, respectively. Intermediates **2** and **3** were obtained by coupling between GCz, DPACz and 3,6-dibromophenanthrene-9,10-dione in yields of 80 and 79%, respectively. The other two final products **2FBP2GCz** and **2FBP2DPACz** were obtained via the cyclization reaction of 4,5-difluorobenzene-1,2-diamine and intermediates **2** and **3**, respectively. The identity and purity of the three emitters was verified by ^{1}H NMR, ^{13}C NMR spectroscopy, melting point determination, high resolution mass spectrometry and elemental analysis and high-performance liquid chromatography (HPLC) (Figures **S1-S28**), with the structure of **2DPACzBP** also being determined by single-crystal XRD.

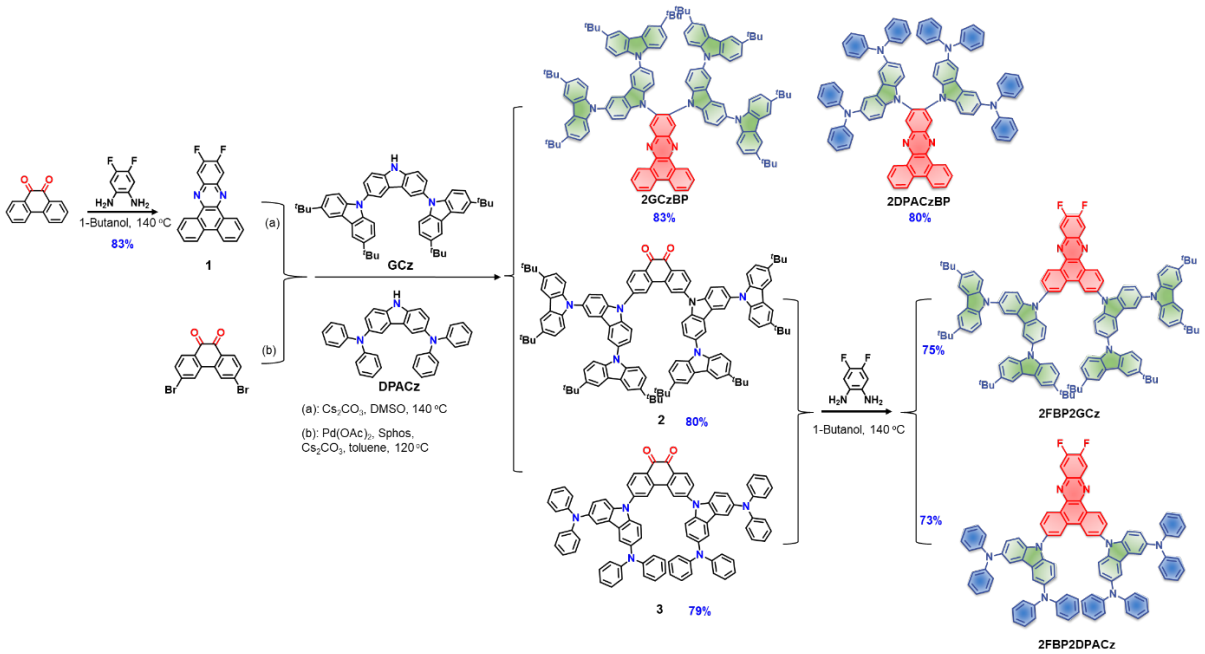

Scheme **1**. Synthetic Routes for **2GCzBP, 2DPACzBP, 2FBP2GCz** and **2FBP2DPACz**.

X-Ray diffraction analysis of 2DPACzBP

Single crystals of **2DPACzBP** were obtained by slow evaporation of a saturated toluene solution at room temperature. **2DPACzBP** adopts a twisted D-A conformation, where the dihedral angles between the BP acceptor and two DPACz donor groups are 62.2° and 65.3° (Figure **2a**). Two different CH···π interactions exist in the compound (Figure **2b**), with H···centroid distances of 2.66 and 2.85 Å [corresponding C···centroid separations of 3.429(6) and 3.700(8) Å]. Each of these gives rise to a centrosymmetric dimer, which combine to form one-dimensional chains along the [1 -1 0] axis. Neighboring molecules also show weak π···π interactions, between the pyrazine and a benzene ring of the BP group [centroid ··· centroid distance of 3.782(3) Å] (Figure **2c**), which result in a weakly-interacting chain along the [0 1 0] axis. The two different sets of interactions combine to give a three-dimensional network, which may contribute to the suppression of non-radiative excitonic transitions.

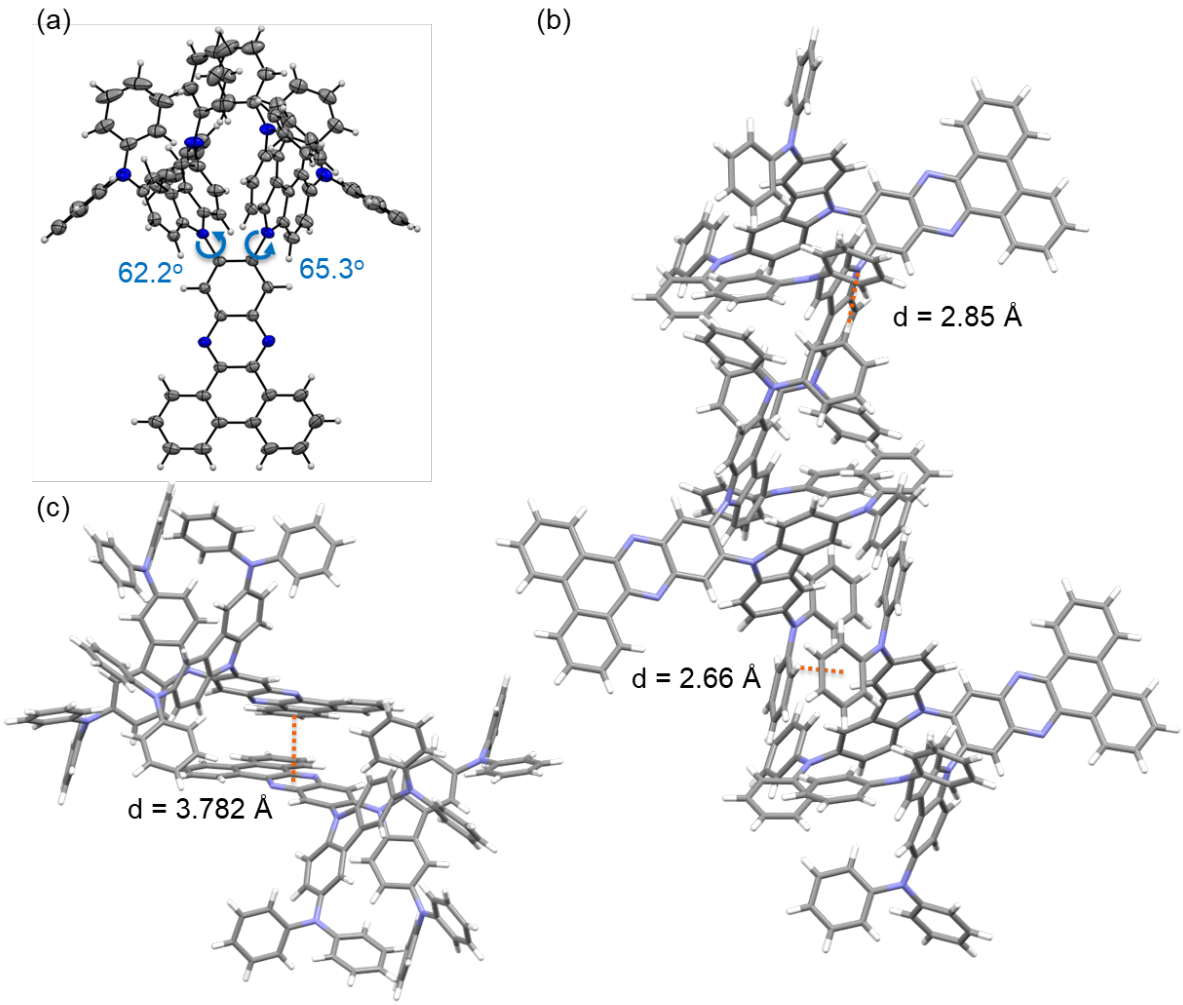

Figure **2**. (a) Thermal ellipsoid plot of one independent molecule in the single crystal structure of **2DPACzBP**. Ellipsoids are drawn at the 50% probability level and solvent molecules has been omitted for clarity; (b) View of CH···π interactions in the compound and (c) view showing π···π interactions between adjacent molecules.

Theoretical Calculations

The ground-state (S_0) geometries of **2GCzBP, 2DPACzBP, 2FBP2GCz** and **2FBP2DPACz** were optimized using Density Functional Theory (DFT) at the PBE0[30]/6-31G(d,p) level[31] in the gas phase starting from a geometry generated in Chem3D.[32] At the optimized S_0 geometries (Figure **S29**), the dihedral angles between the two donors at the 11 and 12 positions and the acceptor moiety in **2GCzBP** (~67°) and **2DPACzBP** (~58°) are much larger than those with the alternative donors at the 3 and 6 positions in **2FBP2GCz** (~43°) and **2FBP2DPACz** (~44°); calculations reproduce the degree of twisting observed in the crystal structure of **2DPACzBP**. This divergence in behavior results from larger steric hindrance between the donors in **2GCzBP**

and **2DPACzBP**. The calculated energy levels of the highest occupied molecular orbitals (HOMOs) and lowest unoccupied molecular orbitals (LUMOs) are shown in Figure **3a** and **S30**. The HOMOs are localized on the donors, while the LUMOs are localized on the BP acceptor group. As the donor strength increases from **2GCzBP** to **2DPACzBP** and from **2FBP2GCz** to **2FBP2DPACz**, the HOMOs are destabilized. As expected, the LUMOs are also destabilized with increasing donor strength from **2GCzBP** to **2DPACzBP** given the electronic coupling between the donor and acceptor groups. When using the same donor, the LUMO of **2GCzBP** is slightly deeper than that of **2FBP2GCz**, this due in part to the two inductively electron-withdrawing fluorine atoms in the acceptor of **2FBP2GCz**. The HOMO of **2GCzBP** (–5.19 eV) is more destabilized compared to that of **2FBP2GCz** (–5.40 eV). This destabilization is attributed to the presence of two donors at adjacent positions exhibiting a cooperative effect, where their combined electronic influence is greater than the sum of their individual effects in **2FBP2GCz**. So, the overall electron-donating ability of **2DPACzBP** is amplified leading to a more destabilized HOMO. The HOMO-LUMO gap, $\Delta E_{HOMO\text{-}LUMO}$, thus decreases from 2.50 eV for **2GCzBP** to 2.38 eV for **2DPACzBP**, while the $\Delta E_{HOMO\text{-}LUMO}$ decreases from 2.72 eV in **2FBP2GCz** to 2.50 eV in **2GCzBP**.

The excited-state properties were calculated using time-dependent DFT (TD-DFT) within the Tamm-Dancoff approximation (TDA-DFT)[33]based on the optimized ground-state geometries (Figure **3b**). The oscillator strength, *f*, for the $S_0 \rightarrow S_1$ transition of **2GCzBP, 2DPACzBP, 2FBP2GCz** and **2FBP2DPACz** is 0.06, 0.01, 0.10 and 0.08, respectively, reflecting the relatively smaller torsions and thus greater conjugation that exist between the position 3, 6 donors and the acceptor moieties in **2FBP2GCz** and **2FBP2DPACz**. The S_1 energies are 2.09 eV for **2GCzBP,** 1.95 eV for **2DPACzBP**, 2.42 eV for **2FBP2GCz** and 2.10 eV for **2FBP2DPACz**, while the corresponding T_1 energies are 2.04 eV, 1.87 eV, 2.32 eV and 2.02 eV, respectively, both following a similar trend to that observed for $\Delta E_{HOMO\text{-}LUMO}$ values (Figure **3a**). All four compounds have small predicted ΔE_{ST} of less than 0.10 eV, suggesting that these compounds should emit via TADF. There is a larger S_1-T_1 spin-orbital coupling matrix element, SOCME, in **2FBP2GCz** (0.19 cm^{-1}) and in **2GCzBP** (0.10 cm^{-1}) than that in **2FBP2DPACz** (0.09 cm^{-1}) and **2DPACzBP** (0.06 cm^{-1}) (Figure **3b**), indicating that the ISC will likely be faster in **2FBP2GCz** and **2GCzBP** than that in the other two compounds. NTO analyses at the S_0-optimized geometry (Figure **3c**) demonstrated that the low-lying excited states in all four compounds possess charge transfer (CT) character. Holes and electrons are well separated on the donor and acceptor moieties, respectively. There is somewhat smaller separation in the T_1 state of **2FBP2GCz** and **2FBP2DPACz**, so this state in these two

compounds is better described as a mixture of locally-excited (LE) and CT character (Figure **3d**).

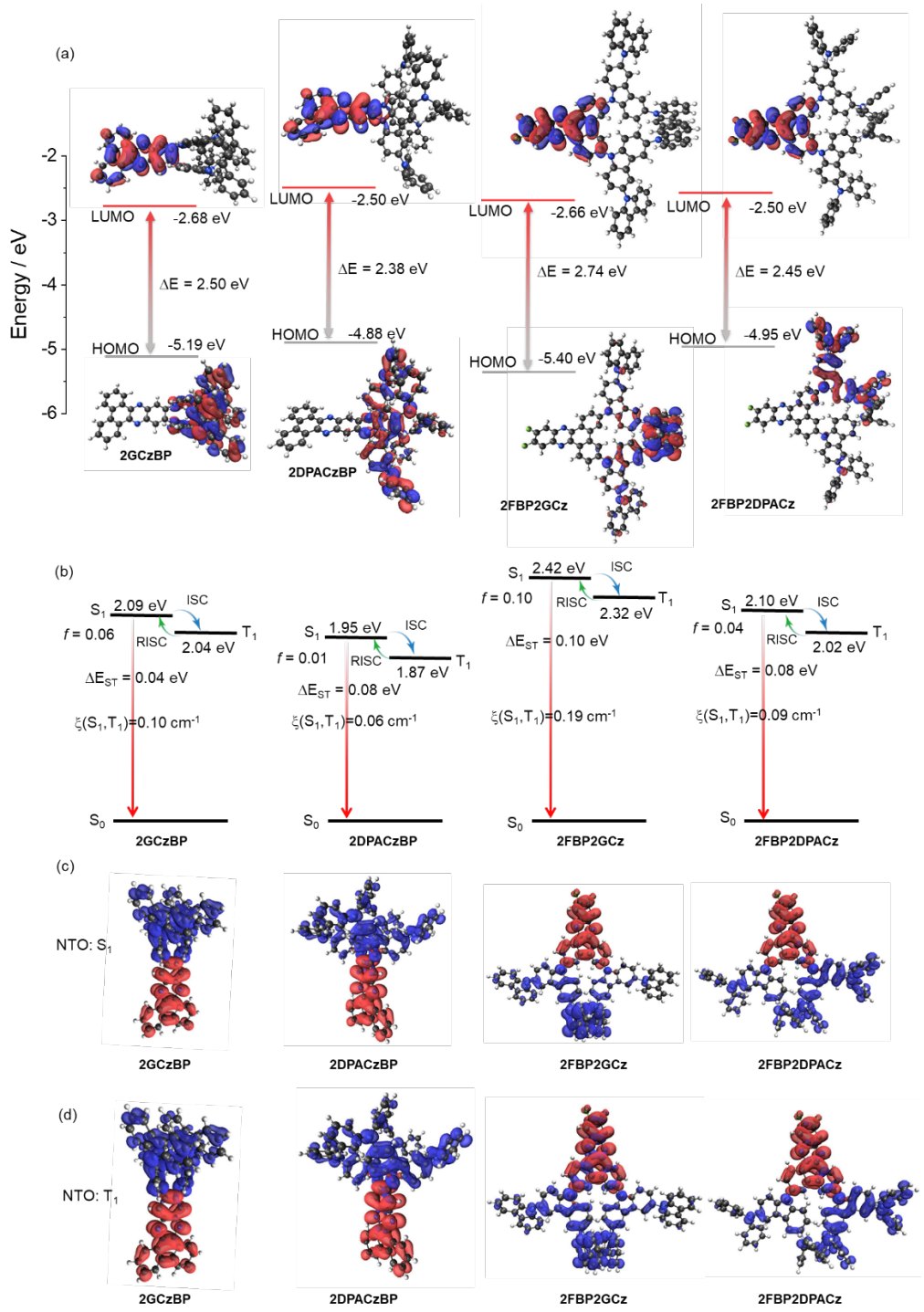

Figure **3**. (a) Frontier molecular orbitals (isovalue: 0.02) and (b) vertical excitation energy levels of **2GCzBP, 2DPACzBP, 2FBP2GCz** and **2FBP2DPACz** calculated at the optimized S_0 geometry in the gas phase at the PBE0/6-31G(d,p) level. Natural transition orbitals (unoccupied (hole, blue) & occupied (electron, red), (isovalue: 0.02)) of (c) S_1 and (d) T_1 for **2GCzBP,**

2DPACzBP, 2FBP2GCz and **2FBP2DPACz** calculated at the optimized S_0 geometry in the gas phase at the PBE0/6-31G(d,p) level.

Electrochemistry

The energies of the frontier molecular orbitals (FMOs) were inferred from the electrochemical behavior of **2GCzBP, 2DPACzBP, 2FBP2GCz** and **2FBP2DPACz** by cyclic voltammetry (CV) and differential pulse voltammetry (DPV) in degassed dichloromethane (DCM) with tetra-*n*-butylammonium hexafluorophosphate, $[^nBu_4N]PF_6$, as the supporting electrolyte (Figure **4a**). The reduction potential (E_{red}), determined from the DPV peak values, are −1.24 (**2GCzBP**), −1.38 (**2DPACzBP**), −1.28 (**2FBP2GCz**) and −1.35 V (**2FBP2DPACz**) reflecting the expected cathodic shift with the increase in donor strength. The LUMO energies are –3.11 eV, −3.07 eV, −3.08 eV and −3.02 eV for **2GCzBP, 2DPACzBP, 2FBP2GCz** and **2FBP2DPACz**, respectively, and align with the trend found for the DFT calculations (Figure **3a**). **2GCzBP** and **2FBP2GCz** both have two resolvable quasi-reversible oxidation waves, with similar first oxidation potentials at E_{ox} of 1.03 V, and second oxidation potentials at 1.13 V, which correspond to the oxidation of the inner carbazole and the peripheral *tert*-butylcarbazole, respectively.[10,34] A similar trend is observed for **2DPACzBP** (E_{ox} = 0.66 V) and **2FBP2DPACz** (E_{ox} = 0.65 V). The HOMO levels of **2GCzBP, 2DPACzBP, 2FBP2GCz** and **2FBP2DPACz** are −5.38, −5.01, −5.37 and −5.02 eV, respectively. The electrochemical data indicate that compounds with the same donors have effectively the same E_{ox}. However, this behavior is not reproduced in the DFT calculations where the calculated HOMO of **2FBP2GCz** (-5.40 eV) is more stabilized than that of **2GCzBP** (-5.19 eV). The corresponding HOMO–LUMO gaps are 2.27, 2.04, 2.30 and 2.00 eV, for **2GCzBP**, **2DPACzBP**, **2FBP2GCz** and **2FBP2DPACz**, respectively, which mirror the trend in the DFT calculated values of 2.50, 2.38, 2.74, 2.45 eV.

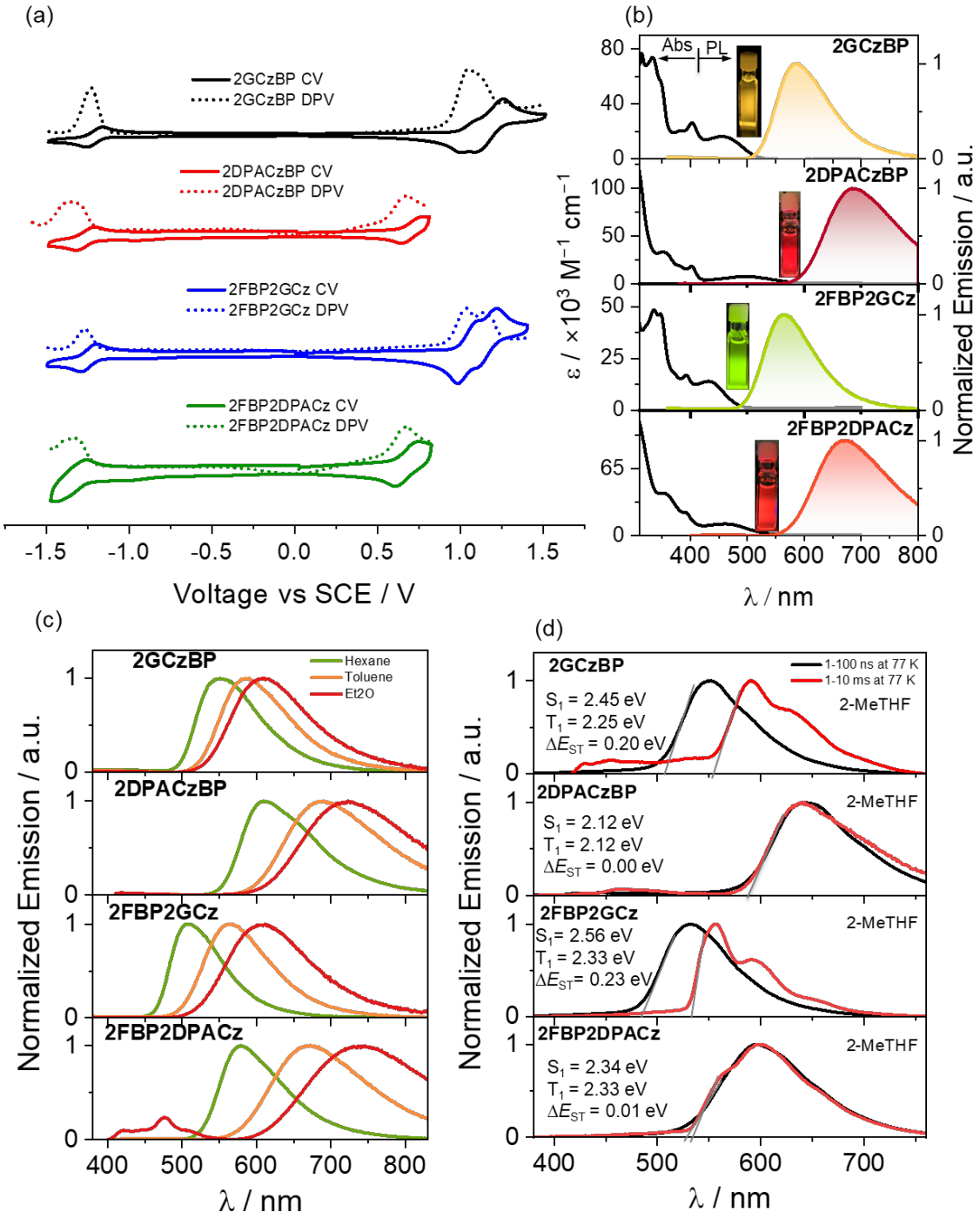

Figure **4**. (a) Cyclic and differential pulse voltammograms measured in degassed DCM with 0.1 M [^{n}Bu$_4$N]PF$_6$ as the supporting electrolyte and Fc/Fc$^+$ as the internal reference (0.46 V vs SCE).[35] Scan rate = 100 mV s^{-1}; (b) UV-vis absorption (in toluene) and steady-state photoluminescence (PL) spectra of **2GCzBP, 2DPACzBP, 2FBP2GCz** and **2FBP2DPACz** recorded in toluene at room temperature (λ_{exc} =340 nm); (c) PL solvatochromism study of **2GCzBP, 2DPACzBP, 2FBP2GCz** and **2FBP2DPACz** recorded at room temperature (λ_{exc} =340 nm); (d) Prompt fluorescence (1-100 ns) and phosphorescence spectra (1-10 ms) in 2-MeTHF at 77 K of **2GCzBP, 2DPACzBP, 2FBP2GCz** and **2FBP2DPACz** (λ_{exc} = 343 nm).

Photophysical Properties

The UV-Vis absorption spectra of the four emitters in dilute toluene are shown in Figure **4b**, and the photophysical properties are summarized in Table **1**. All four compounds exhibit strong absorption bands below 400 nm [**2GCzBP** (346 nm, ε=5.7×10^4 M^{-1} cm^{-1})**, 2DPACzBP** (353 nm, ε=3.3×10^4 M^{-1} cm^{-1})**, 2FBP2GCz** (348 nm, ε=4.7×10^4 M^{-1} cm^{-1}) and **2FBP2DPACz** (354 nm, ε=4.1×10^4 M^{-1} cm^{-1})], which are attributed to LE π–π* transitions of both the donors and acceptor moieties based on a comparison with literature data of BP and GCz.[10,11,27] Weaker and broader absorption bands are observed at 460 nm (ε=1.6×10^4 M^{-1} cm^{-1}) for **2GCzBP**, 506 nm (ε=0.7×10^4 M^{-1} cm^{-1}) for **2DPACzBP**, 436 nm (ε=1.4×10^4 M^{-1} cm^{-1}) for **2FBP2GCz** and 464 nm (ε=1.1×10^4 M^{-1} cm^{-1}) for **2FBP2DPACz**, which are assigned to ICT transitions from the donor units to the acceptor core, assignments that are corroborated by the relative oscillator strengths (f = 0.04, 0.01, 0.10 and 0.04 for **2GCzBP, 2DPACzBP, 2FBP2GCz** and **2FBP2DPACz**, respectively) calculated by TDA-DFT (Figure **3** and **S31**). There is an expected shift to lower energies of the ICT band aligned with increasing donor strength (from **2GCzBP** to **2DPACzBP**) and donor substitution position from position 3 and 6 to position 11 and 12 (**2FBP2GCz** to **2GCzBP**). All compounds exhibit unstructured and broad PL spectra in toluene (Figure **4b**), indicative of an excited state with strong ICT character, with peak maxima, λ_{PL}, at 585, 690, 565, and 675 nm for **2GCzBP, 2DPACzBP, 2FBP2GCz** and **2FBP2DPACz**, respectively. Positive solvatochromism is observed for all compounds (Figure **4c**), which is consistent with the ICT nature of the emissive excited state. The structured higher energy emission band for **2FBP2DPACz** in Et_2O is attributed to originating from an LE state of the donor, as it closely matches the DPACz emission in spectral shape and energy (Figure **S32**). The optical bandgaps, E_g, calculated from the normalized absorption and emission spectra intersection point, are 2.38, 2.09, 2.54, and 2.21 eV for **2GCzBP, 2DPACzBP, 2FBP2GCz** and **2FBP2DPACz**, respectively (Figure **S33**), roughly consistent with the trend in electrochemical redox gaps (Table **1**). The Φ_{PL} values in degassed toluene solution are 59%, 6%, 47% and 9%, respectively, for **2GCzBP, 2DPACzBP, 2FBP2GCz** and **2FBP2DPACz**. When exposed to oxygen, these values significantly decrease to 38% and 27% for **2GCzBP** and **2FBP2GCz**, respectively, and slightly decrease to 5%, and 5% for **2DPACzBP** and **2FBP2DPACz**. The lower Φ_{PL} of **2DPACzBP** and **2FBP2DPACz** may be due in part to the non-radiative decay channels emanating from the more flexible DPACz donor as well as the energy-gap law,[36] which states that the non-radiative decay rate increases exponentially as the energy gap decreases.

The prompt fluorescence and phosphorescence spectra in 2-MeTHF glass at 77 K were measured to determine the S_1 and T_1 energies from their respective onsets (Figure **4d**). The S_1 energies of **2GCzBP, 2DPACzBP, 2FBP2GCz** and **2FBP2DPACz** are 2.45, 2.12, 2.56, and 2.34 eV, and the T_1 energies are 2.25, 2.12, 2.33, and 2.33 eV, respectively. The observed trends for both S_1 and T_1 energy levels align with the computational data presented in Figure **3b.** The phosphorescence spectra of **2GCzBP** and **2FBP2GCz** are structured, and each is assigned from TDA-DFT calculations as a mixed locally excited triplet (^{3}LE) state of the acceptor (BP-F) and charge-transfer (^{3}CT) state (Figure **3d**). The ΔE_{ST} of **2GCzBP, 2DPACzBP, 2FBP2GCz** and **2FBP2DPACz** are 0.20, 0.00, 0.23, and 0.01 eV, respectively, which are similar to the trend in the calculated values, where **2FBP2GCz** has the largest calculated ΔE_{ST} of 0.10 eV compared to **2GCzBP** (0.04 eV)**, 2DPACzBP** (0.08 eV) and **2FBP2DPACz** (0.04 eV), as shown in Figure **3b**.

The PL decays of the four compounds in toluene under degassed conditions were measured using a combination of TCSPC/MCS techniques (Figure **S34**). The ICT bands of **2GCzBP, 2DPACzBP, 2FBP2GCz** and **2FBP2DPACz** all decay with biexponential kinetics, with prompt fluorescence lifetimes, τ_p, of 22.2, 4.2, 14.2, and 3.2 ns, and delayed fluorescence lifetimes, τ_d, of 79.1, 0.24, 102.6, and 0.25 μs, respectively. The corresponding rate constants for intersystem crossing (k_{ISC}) for **2GCzBP, 2DPACzBP, 2FBP2GCz** and **2FBP2DPACz** are 1.0×10^7, 3.9×10^7, 3.0×10^7, and 1.4×10^8 s^{-1}, respectively, while the rate constants for reverse intersystem crossing (k_{RISC}) for **2DPACzBP** (5.0×10^6 s^{-1}) and **2FBP2DPACz** (7.3×10^6 s^{-1}) are much faster than those of **2GCzBP** (1.6×10^4 s^{-1}) and **2FBP2DPACz** (1.4×10^4 s^{-1}), due in part to the smaller ΔE_{ST} in the former two. However, **2DPACzBP** and **2FBP2DPACz** also possess much faster non-radiative decay rate constants (k_{nr}) at 1.9×10^8 and 1.6×10^8 s^{-1}, respectively, than those of **2GCzBP** (k_{nr} =1.4×10^7 s^{-1}) and **2FBP2DPACz** (k_{nr} = 2.1×10^7 s^{-1}), which we attribute to a direct consequence of the energy gap law.[36] The delayed components of **2GCzBP** and **2FBP2GCz** are much longer-lived and were totally quenched by oxygen, reflective of the larger ΔE_{ST} in these two compounds. The corresponding PL intensity of toluene solutions was enhanced upon the oxygen removal for all four compounds (Figure **S34e-f**), demonstrating that oxygen could quench triplet states.

We next assessed the photophysical properties of these emitters in an OLED-relevant host 1,3-bis(*N*-carbazolyl)benzene (mCP), as this host matrix has a sufficiently high triplet energy (T_1 = 2.91 eV) to confine the excitons onto the emitter.[37] Figure **5a** shows the PL spectra of the 1 and 10 wt% doped films in mCP and the neat film. The emission spectra gradually red-shifted by up to 10 nm as the doping concertation increasing from 1 wt% to 10 wt%, while the red-

shift was more pronounced at over 50 nm in neat films due to strong intermolecular interactions.[38] The optimized doping concentration for **2GCzBP**, **2DPACzBP**, **2FBP2GCz** and **2FBP2DPACz** was determined to be 10 wt% as a function of Φ_{PL}, and the corresponding Φ_{PL} values under a N_2 atmosphere are 77, 28, 68, and 44%, respectively, which decrease to 68, 27, 53, and 41%, respectively, under air. The Φ_{PL} values of all four compounds increased compared to those in toluene due to a combination of suppressed non-radiative decay in the solid host and efficient Förster resonance energy transfer (FRET) from host to dopant emitters.[39] The PL spectra of the 10 wt% doped films in mCP, are all unstructured, with λ_{PL} at 570, 640, 560, and 615 nm for **2GCzBP**, **2DPACzBP**, **2FBP2GCz** and **2FBP2DPACz**, respectively (Figure **5a**, Table **1**), values that are slightly blue-shifted compared with those in toluene [**2GCzBP** (585 nm), **2DPACzBP** (690 nm), **2FBP2GCz** (565 nm) and **2FBP2DPACz** (675 nm), Figure **4b**]. It has been demonstrated that the emission color of the compounds is influenced not only by the strength of the donor but also their regiochemistry, undergoing a significant red-shift when the same donors are substituted at positions 11/12 instead of positions 3/6 on the BP acceptor.

The S_1/T_1 energy levels of **2GCzBP** (2.45/2.25 eV)**, 2DPACzBP** (2.12/2.12 eV), **2FBP2GCz** (2.56/2.33 eV) and **2FBP2DPACz** (2.34/2.33 eV) of the 10 wt% doped films in mCP were estimated from the onsets of the fluorescence and phosphorescence spectra at 77 K (Figure **5b**). The corresponding ΔE_{ST} values of **2GCzBP, 2DPACzBP, 2FBP2GCz** and **2FBP2DPACz** are 0.22, 0.01, 0.30, and 0.19 eV, respectively, align with similar results acquired in 2-MeTHF at 77 K. Similar to those in toluene, the fluorescence spectra are all unstructured, indicating emission from ^{1}CT, while the phosphorescence spectra of **2GCzBP** and **2FBP2GCz** are structured, assigned to an emission from the ^{3}LE state of the acceptor. As shown in Figure **5c-d**, all four compounds showed multiexponential decay kinetics with average prompt fluorescence lifetimes, average τ_p, of 22.9, 15.6, 21.1, and 23.0 ns, and average delayed emission lifetimes, average τ_d, of 0.3 ms, 1.3 μs, 3.2 ms and 50.5 μs at room temperature for **2GCzBP, 2DPACzBP, 2FBP2GCz** and **2FBP2DPACz**, respectively. From these average values, the estimated k_{ISC} for the four compounds are 0.52×10^7, 0.23×10^7, 1.12×10^7, and 0.29×10^7 s^{-1} for **2GCzBP, 2DPACzBP, 2FBP2GCz** and **2FBP2DPACz**, respectively, while the estimated k_{RISC} for **2DPACzBP** reached 7.98×10^5 s^{-1}, a value much faster than for **2GCzBP** of 0.36×10^4 s^{-1}, **2FBP2GCz** of 0.04×10^4 s^{-1} and **2FBP2DPACz** of 2.13×10^4 s^{-1}, respectively. Liu *et al.* reported a similar TADF emitter, **TAT-FDBPZ** (Figure **1**), that contains two triazatruxene donors and the same acceptor as **2FBP2GCz/2FBP2DPACz**.[40] **TAT-FDBPZ** emits at λ_{PL} of 593 nm, has a much shorter τ_d of 1.51 μs and faster k_{RISC} of 1.71×10^6 s^{-1} than those of **2FBP2GCz/2FBP2DPACz**, which could result from the more rigid and

conjugated structure of TAT than those of GCz and DPACz used in our work. For the same donor, the k_{RISC} for the compounds substituted in 11/12 positions is more than 10-times faster than that of the compounds substituted in 3/6 positions, due to the smaller ΔE_{ST}. For compounds with the same substitution pattern, the k_{RISC} for the compounds substituted by the stronger DPACz donors is more than 50 times faster than that of compounds with weaker GCz donors due to its smaller ΔE_{ST}. Xie *et al.* reported a TADF molecule, **2DMAC-BP**, containing two DMAC donors attached to the BP acceptor,[41] which emits at λ_{PL} of 553 nm, has a τ_d of 7.5 μs and k_{RISC} of 4.74×10^5 s^{-1} in 20 wt% doped films in mCBP, thereby having a k_{RISC} that is around half that of **2DPACzBP** ($k_{RISC} = 7.98 \times 10^5$ s^{-1}). Zeng *et al.* developed another TADF emitter **DPPZ-2DMAC**, which consists of a similar acceptor to BP and two DMAC donors substituted at the 10 and 11 positions.[42] Similar to what was observed in **2DMAC-BP**, **DPPZ-2DMAC** exhibits a red-shifted emission of λ_{PL}= 620 nm and has shorter τ_d of 4.5 μs and fast k_{RISC} of 5.52×10^5 s^{-1} that is nonetheless slower than that of **2DPACzBP**. Finally, as shown in Figure **5c-d**, the relative intensities of the delayed PL increase with increasing temperature from 100 K to 300 K, thereby corroborating the TADF nature of the emission of these four compounds in the 10 wt% films in mCP.

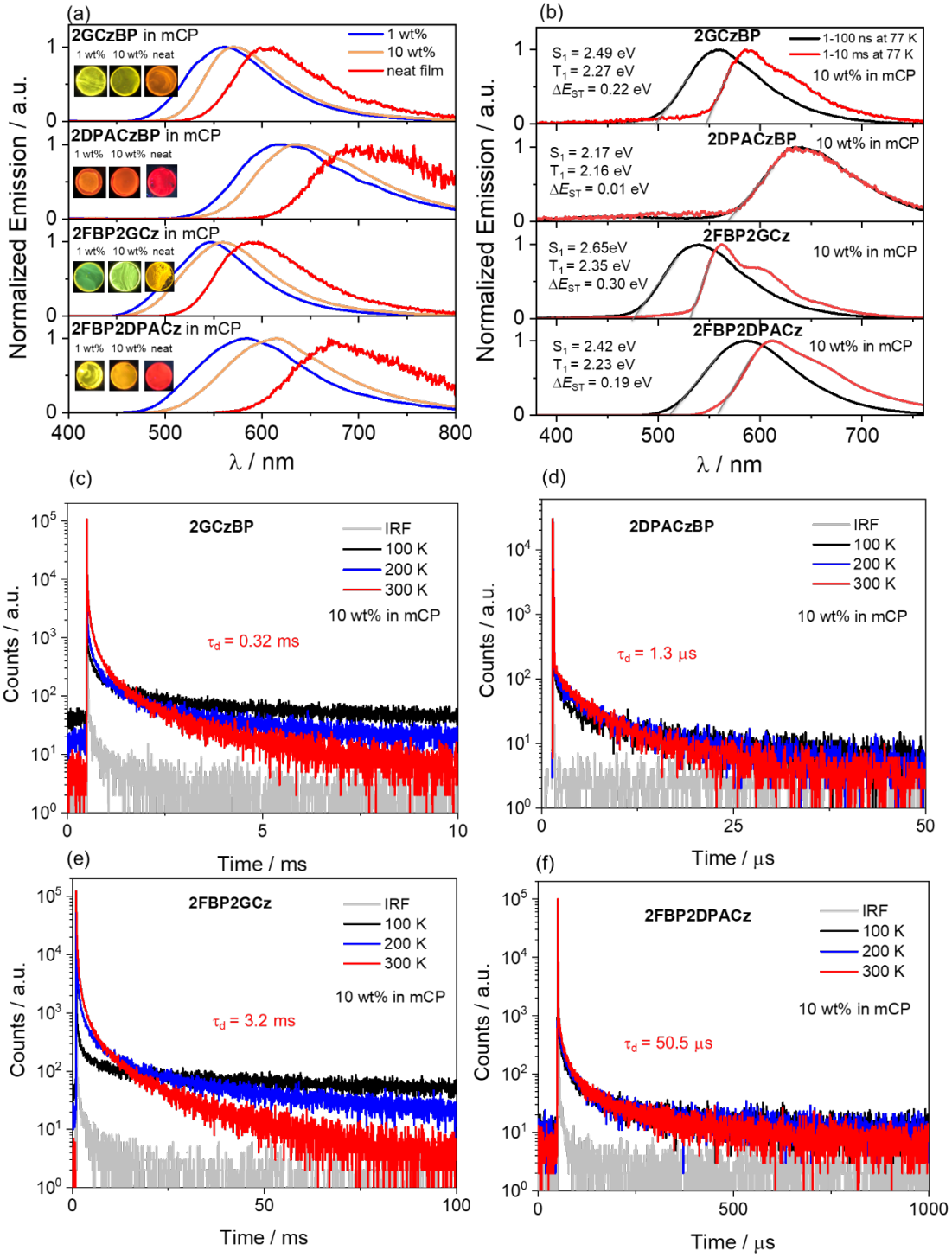

Figure **5.** (a) Steady-state PL spectra of **2GCzBP, 2DPACzBP, 2FBP2GCz** and **2FBP2DPACz** recorded in doped mCP film at room temperature (λ_{exc} = 340 nm). (b) Prompt fluorescence (1-100 ns) and phosphorescence spectra (1-10 ms) in 10 wt% doped films in mCP at 77 K of **2GCzBP, 2DPACzBP, 2FBP2GCz** and **2FBP2DPACz** (λ_{exc} = 343 nm). Temperature-dependent time-resolved PL decay of 10 wt% (c) **2GCzBP**, (d) **2DPACzBP,** (e) **2FBP2GCz** and (f) **2FBP2DPACz** doped films in mCP (λ_{exc}= 379 nm).

Table **1.** Photophysical properties of **2GCzBP**, **2DPACzBP**, **2FBP2GCz** and **2FBP2DPACz**.

	λ_{abs}/(ε / $\times10^3$ M^{-1} cm^{-1}) [a] / nm	λ_{PL} [a] / nm	S_1/T_1 [b] / eV	ΔE_{ST} [b] / eV	λ_{PL} [c] / nm	Φ_{PL} [c] / %	τ_p [d] / ns	τ_d [d] / μs	S_1/T_1 [e] / eV	ΔE_{ST} / eV	k_{ISC} [f] /$\times10^7$ s^{-1}	k_{RISC} [f] /$\times10^4$ s^{-1}	k_{s_r} [f] /$\times10^7$ s^{-1}	k_{s_nr} [f] /$\times10^7$ s^{-1}	HOMO[g] /eV	HOMO[g] /eV	Eg[h]/ eV
2GCzBP	346 (57), 460(16)	585	2.45/ 2.25	0.20	570	77 (68)	22.9	317	2.49/ 2.27	0.22	0.52	0.36	2.96	0.88	-5.38	-3.11	2.27
2DPACzBP	353 (33), 403(18), 506(7)	690	2.12/ 2.12	0.00	640	28 (27)	15.6	1.3	2.17/ 2.16	0.01	0.23	79.8	1.73	4.45	-5.01	-2.97	2.04
2FBP2GCz	348 (47), 394(17), 436(14)	565	2.56/ 2.33	0.23	560	68 (53)	21.1	3200	2.65/ 2.35	0.30	1.12	0.04	2.51	1.18	-5.37	-3.07	2.30
2FBP2DPACz	354(41), 394(22), 464(11)	675	2.35/ 2.30	0.05	615	44 (41)	23.0	50.5	2.42/ 2.23	0.19	0.29	2.13	1.78	2.27	-5.02	-3.02	2.00

[a] In PhMe at 298 K (λ_{exc}=340 nm). [b] Obtained from the onset of the prompt fluorescence (time window: 1 ns – 100 ns) and phosphorescence spectra (time window: 1 ms – 10 ms) measured in 2-MeTHF glass at 77 K, λ_{exc} = 343 nm. [c] Thin films of 10wt% emitters doped in mCP were prepared by spin-coating. and Φ_{PL} values were determined using an integrating sphere (λ_{exc}=340 nm). Values quoted are under N_2. Values in parentheses are in air. [d] Average lifetime ($\tau_{avg} = \Sigma A_i\tau_i^2 / \Sigma A_i\tau_i$, where A_i is the pre-exponential for lifetime τ_i). PL lifetimes were measured by TCSPC and MCS, respectively (λ_{exc} = 379 nm). [e] S_1 was obtained from the onset of the prompt emission (time-gated window: 1–100 ns) ms measured in doped film at 77 K and T_1 was obtained from the onset of the phosphorescence spectrum (time-gated window: 1–10 ms) measured in doped film at 77 K. [f] k_{ISC} = intersystem crossing rate from S_1 to T_1 states; k_{RISC} = reverse intersystem crossing rate. [g] In DCM with 0.1 M [^{n}Bu$_4$N]PF_6 as supporting electrolyte and Fc/Fc^+ as the internal reference (0.46 V vs. SCE).[35] The HOMO and LUMO energies were determined using $E_{HOMO/LUMO}$= - (E_{ox}/ E_{red} +4.8) eV where E_{ox} and E_{red} are anodic and cathodic peak potentials, respectively, obtained from the DPV.[35] [h] E_g= $|E_{HOMO}-E_{LUMO}|$.

Device characterization

To evaluate the electroluminescent (EL) performance of these emitters, solution-processed OLEDs employing 10 wt% emitters doped in mCP films as the emissive layer (EML) were fabricated with a typical configuration of indium ITO (indium tin oxide)/ poly(3,4-ethylenedioxythiophene):poly(styrenesulfonate) (PEDOT:PSS) (40 nm)/ mCP : 10 wt% dopant (20 nm)/TmPyPB (3,3′-(5′-(3-(pyridin-3-yl)phenyl)-[1,1′:3′,1″-terphenyl]-3,3″-diyl)dipyridine) (45 nm)/LiF (1 nm)/Al (Figure **6** and **S35**), where ITO and Al serve as the anode and cathode, respectively. PEDOT:PSS and TmPyPB are sequentially used as the hole-transporting layer and electron-transporting layer, respectively. As shown in Figure **S35**, the OLEDs with **2FBP2GCz, 2GCzBP**, **2FBP2DPACz** and **2DPACzBP** at doping concertation of 10 wt% in mCP host exhibit green, yellow to pure red emission with the electroluminescence peaks, λ_{EL}, at 545, 561, 585 and 640 nm, and corresponding Commission Internationale de L'Éclairage (CIE) coordinates of (0.37, 0.57), (0.46, 0.53), (0.51, 0.48) and (0.61, 0.36) in the device, which match the PL emission very well (Figures **5a**). As depicted in Figure **6b**, the devices with **2DPACzBP** showed the highest EQE_{max} of 7.8% at 600 cd m^{-2} (Figure **7a**) and negligible efficiency roll-off at 1000 cd m^{-2} (EQE_{1000}= 7.6%), which is the highest EQE_{1000} in reported red solution-processed OLEDs to date (Figure **7b** and Table **2** and **S1**), and maintains 87% of its EQE_{max} at 2000 cd m^{-2} (EQE_{2000}= 6.8%).

To improve the efficiency of the devices, we next explored the fabrication of TADF-sensitized-fluorescence, or hyperfluorescence (HF), devices (Figure **6a**).[43] Here, **4CzIPN** was selected as the TADF assistant dopant because of its high Φ_{PL}, short τ_d in mCP, [44–46] and a strong spectral overlap between the absorption spectra of these four emitters and the PL spectrum of **4CzIPN** in toluene (Figure **S36**). The optimized ratio of emitters/4CzIPN/ mCP was established in the literature to be 3: 32: 65.[43,47,48] The device performance is shown in Figure **6c-e**, and the data are summarized in Table **2**. As shown in Figure **6e**, the EQEs of the HF devices with all four compounds have been greatly improved compared to the previous set of devices. The HF devices with **2DPACzBP** showed an enhanced EQE_{max} of 20.0% at λ_{EL}= 605 nm (Figure **7a**), much higher than 7.8% in the non-HF devices. However, a noticeable blue-shift in the EL spectra was observed, moving from λ_{EL} = 640 nm (no-HF devices) to λ_{EL}= 605 nm in HF devices, which we attributed to the lower doping concertation of emitter in the EML. The HF devices with **2FBP2GCz, 2GCzBP** and **2FBP2DPACz** showed higher EQE_{max} of 18.7, 13.5 and 17.0% with blue-shifted EL spectra λ_{EL} at 540, 555 and 580, respectively, than their respective non-HF devices. The EQE_{1000} in the HF devices with **2FBP2GCz, 2GCzBP**,

2FBP2DPACz and **2DPACzBP** still remained reasonably high at 17.3%, 12.3%, 16.8% and 11.8%, respectively (Table **2**), which, to the best of our knowledge, is amongst the best performance for orange to red HF SP-OLED to date (Figure **7**).

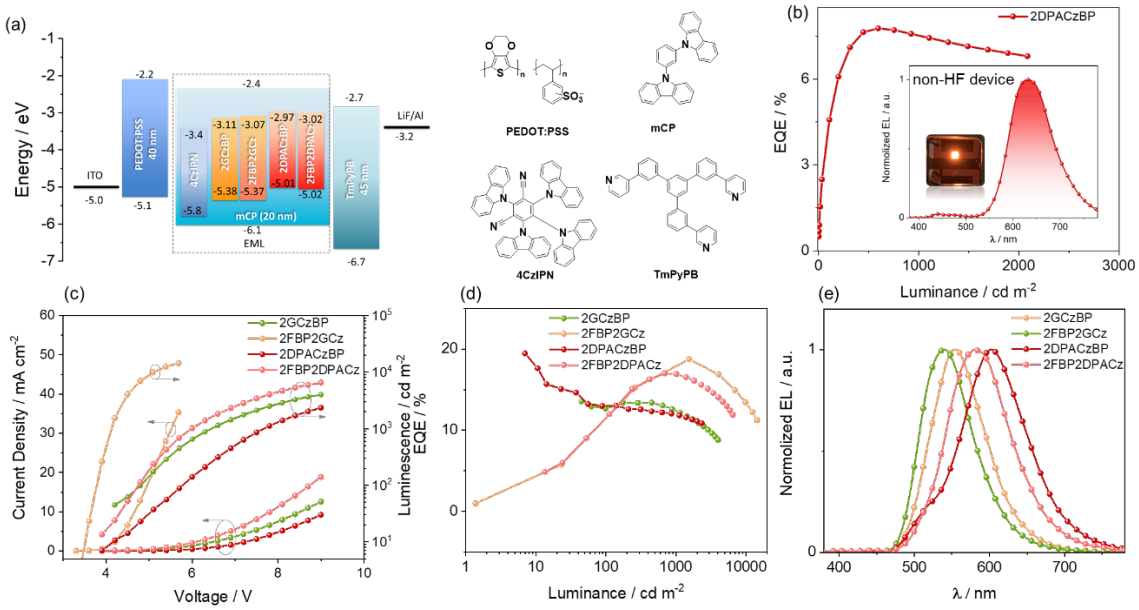

Figure **6**. (a) Energy level diagram and molecular structure of materials of materials employed in the HF devices; (b) External quantum efficiency versus luminance curves and EL spectra of for **2DPACzBP** based device with the structure of ITO/PEDOT:PSS (40 nm)/ mCP:10 wt% dopants (20 nm)/TmPyPB (45 nm)/LiF (1 nm)/Al; (c) Current density and luminance versus voltage characteristics for the HF devices; (d) external quantum efficiency versus luminance curves for the HF devices; (e) electroluminescence spectra of the HF devices.

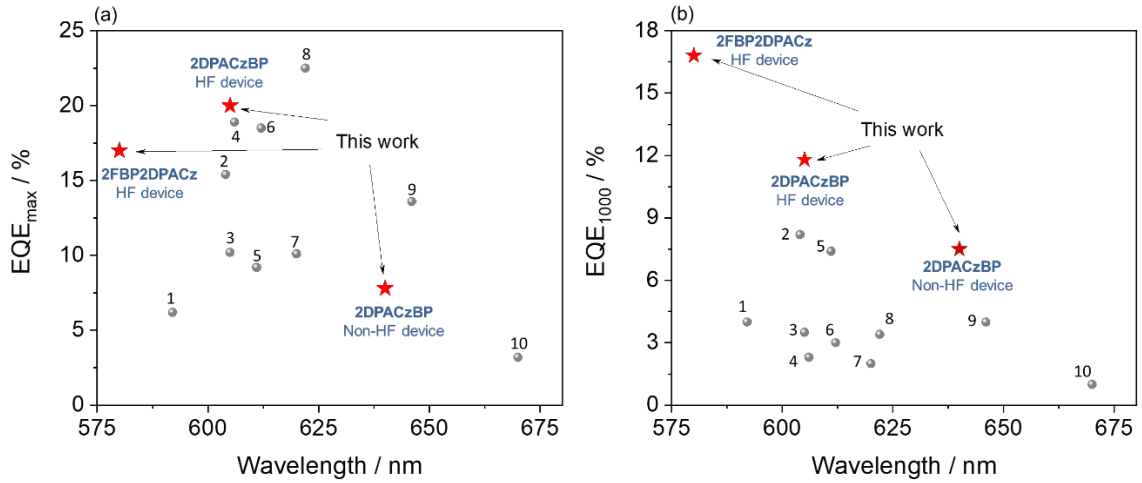

Figure 7. (a) The maximum EQE values and (b) The EQE values at 1000 cd m^{-2} of all reported orange-to-red solution-processed (λ_{EL}> 575 nm) TADF OLEDs as a function of wavelength. (see Table **S1** in ESI).

Table **2**. Electroluminescence data for the devices

Emitter	Host	V_{on}[a] / V	λ_{EL}[b] / nm	CE / cd A^{-1}	PE_{max} / lm W^{-1}	EQE[c] / %	CIE[d] / x,y
2GCzBP	mCP (10%)	3.9	561	8.8	3.1	2.7/1.1/2.3	0.46, 0.53
2FBP2GCz	mCP (10%)	3.0	545	10.3	3.8	3.1/1.0/2.6	0.37, 0.57
2DPACzBP	mCP (10%)	3.4	640	9.6	4.9	7.8/4.6/7.5	0.61, 0.36
2FBP2DPACz	mCP (10%)	3.2	585	10.8	3.8	4.0/1.4/3.2	0.51, 0.48
2GCzBP	mCP:4CzIPN(65%:32%) (3%)	3.9	555	49.0	36.6	13.5/13.1/12.3	0.41, 0.57
2FBP2GCz	mCP:4CzIPN(65%:32%) (3%)	3.0	540	68.2	51.0	18.7/11.2/17.3	0.34, 0.60
2DPACzBP	mCP:4CzIPN(65%:32%) (3%)	3.4	605	46.1	36.7	20.0/13.1/11.8	0.53, 0.45
2FBP2DPACz	mCP:4CzIPN(65%:32%) (3%)	3.2	580	49.5	27.3	17.0/11.3/16.8	0.49, 0.49

[a] The turn-on voltage at a brightness ≈ 1 cd m^{-2}. [b] The electroluminescence maximum recorded at 6 V. [c] EQE_{max}/EQE_{100}/ EQE_{1000}. [d] The CIE coordinates recorded at 6 V.

Conclusions

Here, we designed and synthesized four novel orange-red solution-processable TADF dendrimers, **2GCzBP**, **2DPACzBP**, **2FBP2GCz** and **2FBP2DPACz**. We systematically investigated the effect of substitution position and strength of the donors on their optoelectronic

properties. From this study we could draw the following conclusions: 1). The emission color of the compounds not only depends on the donor strength but also shows a large red-shift when same donors are substituted from position 3/6 to position 11/12 of the BP acceptor; 2). The k_{RISC} for the compounds substituted in positions 11 and 12 of BP is more than ten times faster than that of compounds substituted in positions 3 and 6; 3). **2GCzBP** exhibits the highest Φ_{PL} of 77%, the Φ_{PL} slightly decease to 68% for **2FBP2GCz**, wherein both compounds have donors at the 3 and 6 positions. However, both **2DPACzBP** and **2FBP2DPACz** have much lower Φ_{PL}**,** which we attribute to a consequence of the energy gap law, especially for **2DPACzBP** (the smallest S_1 and lowest Φ_{PL}); 4). Due to the larger dihedral angles between the donors at the 11/12 positions and the acceptor, **2GCzBP** and **2DPACzBP** possess much smaller ΔE_{ST} compared to their respective analogs, **2FBP2GCz** and **2FBP2DPACz**. Furthermore, the stronger donor contributes to the smaller ΔE_{ST} in these compounds with the same substitution position. The SP-OLED with **2DPACzBP** emitted at λ_{EL}= 640 nm and showed an EQE_{max} of 7.8% and a low efficiency roll-off where the EQE remains high at 7.5% at a luminance of 1000 cd m^{-2}, which is among the best results for red solution-processed TADF OLEDs at this luminance. The much worse performance for the devices with **2GCzBP**, **2FBP2GCz** and **2FBP2DPACz** may be linked to a combination of their slower k_{RISC} and their having an unoptimized device structure. The efficiency of the HF devices using **4CzIPN** as the assistant dopant improved significantly, where the **2DPACzBP** HF device showing a particularly attractive performance with an EQE_{max} of 20.0% at λ_{EL} = 605 nm, which is the best performance for the orange-to-red HF SP-OLED.

Acknowledgments

Changfeng Si thanks the China Scholarship Council (201806890001). Dianming Sun acknowledges support from the Royal Academy of Engineering Enterprise Fellowship (EF2122-13106). We thank EPSRC (grants EP/W015137/1 and EP/W524505/1) for financial support.

Conflict of Interest

The authors declare no conflict of interest.

Supporting Information

TOC Graphic

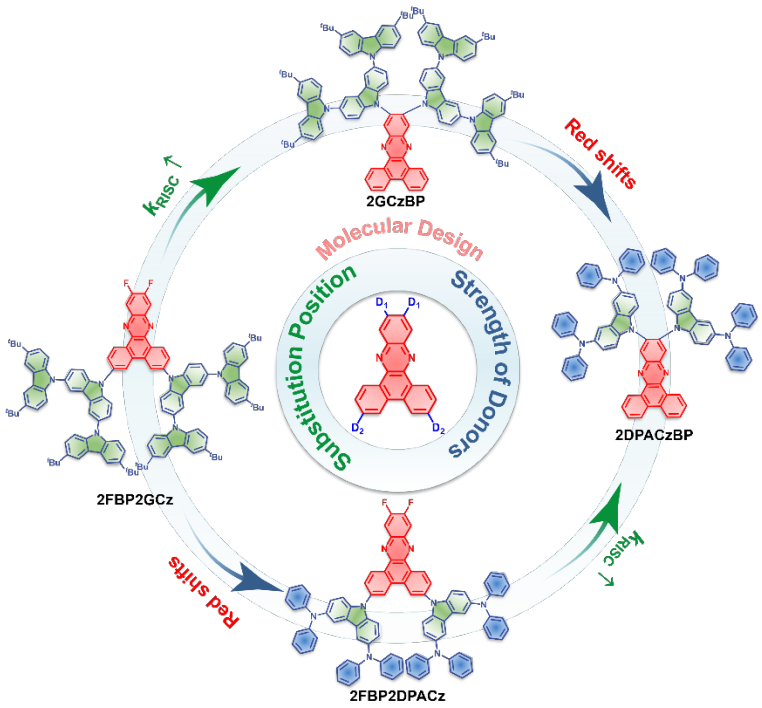

References

1 D. Sun, C. Si, T. Wang and E. Zysman-Colman, *Adv. Photonics Res.*, 2022, 2200203.

2 S. J. Zou, Y. Shen, F. M. Xie, J. De Chen, Y. Q. Li and J. X. Tang, *Mater. Chem. Front.*, 2020, 4, 788–820.

3 T. Huang, W. Jiang and L. Duan, *J. Mater. Chem. C*, 2018, 6, 5577–5596.

4 M. Y. Wong and E. Zysman-Colman, *Adv. Mater.*, 2017, **29**, 1605444.

5 H. Uoyama, K. Goushi, K. Shizu, H. Nomura and C. Adachi, *Nature*, 2012, **492**, 234–238.

6 N. Thejo Kalyani and S. J. Dhoble, *Renew. Sustain. Energy Rev.*, 2012, **16**, 2696–2723.

7 S. Wang, H. Zhang, B. Zhang, Z. Xie and W. Y. Wong, *Mater. Sci. Eng. R Reports*, 2020, **140**, 100547.

8 Y. Xie and Z. Li, *J. Polym. Sci. Part A Polym. Chem.*, 2017, **55**, 575–584.

9 H. Uoyama, K. Goushi, K. Shizu, H. Nomura and C. Adachi, *Nature*, 2012, **492**, 234–238.

10 D. Sun, E. Duda, X. Fan, R. Saxena, M. Zhang, S. Bagnich, X. Zhang, A. Köhler and E. Zysman-Colman, *Adv. Mater.*, 2022, **34**, 2110344.

11 D. Sun, R. Saxena, X. Fan, S. Athanasopoulos, E. Duda, M. Zhang, S. Bagnich, X. Zhang, E. Zysman-Colman and A. Köhler, *Adv. Sci.*, 2022, **9**, 2201470.

12 A. S. Abd-El-Aziz, A. A. Abdelghani, B. D. Wagner and R. Bissessur, *Macromol. Rapid Commun.*, 2019, **40**, 58–61.

13 K. Albrecht, K. Matsuoka, K. Fujita and K. Yamamoto, *Angew. Chemie - Int. Ed.*, 2015, **54**, 5677–5682.

14 P. L. Burn, S. C. Lo and I. D. W. Samuel, *Adv. Mater.*, 2007, **19**, 1675–1688.

15 G. Zhao, D. Liu, P. Wang, X. Huang, H. Chen, Y. Zhang, D. Zhang, W. Jiang, Y. Sun and L. Duan, *Angew. Chemie Int. Ed.*, 2022, **61**, e202212861.

16 S. Zeng, C. Xiao, J. Zhou, Q. Dong, Q. Li, J. Lim, H. Ma, J. Y. Lee, W. Zhu and Y. Wang, *Adv. Funct. Mater.*, 2022, **32**, 2113183.

17 J. Liu, L. Chen, X. Wang, Q. Yang, L. Zhao, C. Tong, S. Wang, S. Shao and L. Wang, *Macromol. Rapid Commun.*, 2022, **43**, 2200079.

18 Y. H. Kim, C. Wolf, H. Cho, S. H. Jeong and T. W. Lee, *Adv. Mater.*, 2016, **28**, 734–741.

19 Y. Wada, S. Kubo and H. Kaji, *Adv. Mater.*, 2018, **30**, 1705641.

20 J. S. Wilson, N. Chawdhury, M. R. A. Al-Mandhary, M. Younus, M. S. Khan, P. R. Raithby, A. Köhler and R. H. Friend, *J. Am. Chem. Soc.*, 2001, **123**, 9412–9417.

21 J. V. Caspar, E. M. Kober, B. P. Sullivan and T. J. Meyer, *J. Am. Chem. Soc.*, 1982, **104**, 630–632.

22 Y. J. Yu, Y. Hu, S. Y. Yang, W. Luo, Y. Yuan, C. C. Peng, J. F. Liu, A. Khan, Z. Q. Jiang and L. S. Liao, *Angew. Chemie - Int. Ed.*, 2020, **59**, 21578–21584.

23 X. Li, K. Wang, Y. Z. Shi, M. Zhang, G. Le Dai, W. Liu, C. J. Zheng, X. M. Ou and X. H. Zhang, *J. Mater. Chem. C*, 2018, **6**, 9152–9157.

24 Y. Zhang, J. Wu, J. Song, Z. Chen, J. He, X. Wang, H. Liu, S. Chen, J. Qu and W. Y. Wong, *Adv. Electron. Mater.*, 2019, **5**, 1800677.

25 B. Wang, H. Yang, Y. Zhang, G. Xie, H. Ran, T. Wang, Q. Fu, Y. Ren, N. Sun, G. Zhao, J. Y. Hu and Q. Wang, *J. Mater. Chem. C*, 2019, **7**, 12321–12327.

26 W. Zeng, T. Zhou, W. Ning, C. Zhong, J. He, S. Gong, G. Xie and C. Yang, *Adv. Mater.*, 2019, **31**, 1901404.

27 J. Chen, Y. Xiao, K. Wang, D. Sun, X. Fan, X. Zhang, M. Zhang, Y. Shi, J. Yu, F. Geng, C. Lee and X. Zhang, *Angew. Chemie Int. Ed.*, 2021, **60**, 2478–2484.

28 S. Sharma and A. K. Pal, *J. Mater. Chem. C*, 2022, 10, 15681–15707.

29 J. H. Kim, J. H. Yun and J. Y. Lee, *Adv. Opt. Mater.*, 2018, **6**, 1800255.

30 C. Adamo and V. Barone, *J. Chem. Phys.*, 1999, **110**, 6158–6170.

31 G. A. Petersson, T. G. Tensfeldt and J. A. Montgomery, *J. Chem. Phys.*, 1991, **94**, 6091–6101.

32 S. M. Kerwin, *J. Am. Chem. Soc.*, 2010, **132**, 2466–2467.

33 S. Hirata and M. Head-Gordon, *Chem. Phys. Lett.*, 1999, **314**, 291–299.

34 E. Duda, D. Hall, S. Bagnich, C. L. Carpenter-Warren, R. Saxena, M. Y. Wong, D. B. Cordes, A. M. Z. Slawin, D. Beljonne, Y. Olivier, E. Zysman-Colman and A. Köhler, *J. Phys. Chem. B*, 2022, **126**, 552–562.

35 N. G. Connelly and W. E. Geiger, *Chem. Rev.*, 1996, **96**, 877–910.

36 R. Englman and J. Jortner, *Mol. Phys.*, 1970, **18**, 145–164.

37 W. Zeng, T. Zhou, W. Ning, C. Zhong, J. He, S. Gong, G. Xie and C. Yang, *Adv. Mater.*, 2019, **31**, 1901404.

38 J. Xue, Q. Liang, R. Wang, J. Hou, W. Li, Q. Peng, Z. Shuai and J. Qiao, *Adv. Mater.*, 2019, **31**, 1808242.

39 L. Wu, C. Huang, B. P. Emery, A. C. Sedgwick, S. D. Bull, X. P. He, H. Tian, J. Yoon, J. L. Sessler and T. D. James, *Chem. Soc. Rev.*, 2020, 49, 5110–5139.

40 Y. Liu, Y. Chen, H. Li, S. Wang, X. Wu, H. Tong and L. Wang, *ACS Appl. Mater. Interfaces*, 2020, **12**, 30652–30658.

41 F. M. Xie, H. Z. Li, G. L. Dai, Y. Q. Li, T. Cheng, M. Xie, J. X. Tang and X. Zhao, *ACS Appl. Mater. Interfaces*, 2019, **11**, 26144–26151.

42 X. Zeng, J. Zhou, S. Zou, Y. Tang, H. Li, Y. He, Y. Li, W. Wang and J. Tang, *Adv. Opt. Mater.*, 2022, **10**, 2200277.

43 C. Y. Chan, M. Tanaka, Y. T. Lee, Y. W. Wong, H. Nakanotani, T. Hatakeyama and C. Adachi, *Nat. Photonics*, 2021, **15**, 203–207.

44 J. W. Sun, J. H. Lee, C. K. Moon, K. H. Kim, H. Shin and J. J. Kim, *Adv. Mater.*, 2014, **26**, 5684–5688.

45 S. Wu, A. Kumar Gupta, K. Yoshida, J. Gong, D. Hall, D. B. Cordes, A. M. Z. Slawin, I. D. W. Samuel and E. Zysman-Colman, *Angew. Chemie Int. Ed.*, 2022, **61**, e202213697.

46 H. S. Kim, S. R. Park and M. C. Suh, *J. Phys. Chem. C*, 2017, **121**, 13986–13997.

47 D. Chen, X. Cai, X. L. Li, Z. He, C. Cai, D. Chen and S. J. Su, *J. Mater. Chem. C*, 2017, **5**, 5223–5231.

48 J. Y. Woo, M. Park, S. Jeong, Y. Kim, B. Kim, T. Lee and T. Han, *Adv. Mater.*, 2023, **35**, 2207454.